Investigation of Limits to the Optical Performance of Asymmetric Fabry-Perot Electroabsorption Modulators

Ross M. Audet, *Student Member, IEEE*, Elizabeth H. Edwards, *Member, IEEE*, Pierre Wahl, and David A. B. Miller, *Fellow, IEEE*

***Abstract*— We have investigated the suitability of surface-normal asymmetric Fabry-Perot electroabsorption modulators for short-distance optical interconnections between silicon chips. These modulators should be made as small as possible to minimize device capacitance; however, size-dependent optical properties impose constraints on the dimensions. We have thus performed simulations that demonstrate how the optical performance of the modulators depends on both the spot size of the incident beam and the dimensions of the device. We also discuss the tolerance to nonidealities such as surface roughness and beam misalignment. The particular modulators considered here are structures based upon the quantum-confined Stark effect in Ge/GeSi quantum wells. We present device designs that have predicted extinction ratios greater than 7 dB and switching energies as low as 10 fF/bit, which suggests that these silicon-compatible devices can enable high interconnect bandwidths without the need for wavelength division multiplexing.**

***Index Terms*— Integrated optoelectronics, optical interconnections, optical modulation, optical resonators.**

I. Introduction

A. Background

THERE are many present efforts to develop optical modulators for short distance inter- and intra-chip optical interconnects [1], since the performance of electrical links, measured in terms of bandwidth and power consumption, has failed to improve at the same rate as transistor performance with successive generations of complementary metal-oxide semiconductor (CMOS) technology [2]. Optical interconnects could help alleviate the interconnect bottleneck in computer systems and facilitate new architectures for high-performance computing [3], [4], provided the optical devices are sufficiently energy-efficient [5].

Integrated optical modulators are either waveguide or surface-normal devices. In the former, modulation and guiding of light occurs in the plane of the chip. With surface-normal modulators, however, the incident and reflected beams are perpendicular to the chip surface. While both geometries have various merits, we focus here on surface-normal modulators, as they have a number of attractive features, particularly for inter-chip links, such as low insertion loss, polarization independence, and relatively easy alignment compared to waveguide devices. Additionally, the reflection-mode geometry is compatible with dense 2-D array integration. Such dense arrays make it possible to create links with large numbers of channels (e.g., 1000s to 10 000s). As a result, surface-normal devices can provide continued scaling of interconnect bandwidth to chips well beyond what is possible with simple waveguide approaches [5], and without the complexity of wavelength division multiplexing schemes.

There have been a number of successful experimental demonstrations of highly parallelized free-space optical links [6], [7]. In these demonstrations, light incident from an external source is imaged onto an array of modulators using an intermediate layer of optics, and the same optics direct the reflected light to photodetectors in other areas of the chips. Large parallel optically connected logic systems based on III–V devices have been successfully demonstrated with over 60 000 light beams [8].

The most efficient reflection modulators are quantum well electroabsorption modulators with asymmetric Fabry-Perot (AFP) cavities [9]–[13]. The electroabsorption mechanism in these asymmetric Fabry-Perot modulators (AFPMs) is the quantum-confined Stark effect (QCSE) [14]. The AFP cavity enables a large change in the reflected power given only a modest change in the material absorption, yielding high contrast ratios even for small voltage swings. While QCSE AFPMs have historically been made from III–V materials, recent progress in the growth [15], [16] and modeling [17], [18] of germanium quantum wells on silicon substrates has enabled the fabrication of QCSE electroabsorption modulators in a CMOS-compatible material system [19], [20].

In any modulator, it is desirable to maximize the speed and contrast ratio while minimizing the energy consumption and

Manuscript received July 27, 2011; revised August 30, 2011; accepted September 2, 2011. Date of current version January 24, 2012. This work was supported in part by the Defense Advanced Research Projects Agency (DARPA) under Agreement HR0011-08-09-0001 between Oracle and the Government, and the DARPA Microsystems Technology Office Seedling Program, the Semiconductor Research Corporation Focus Center Research Program Interconnect Focus Center, the Robert Bosch Corporation Stanford Graduate Fellowship, and the Belgian American Education Foundation. This work was funded in part by the U.S. Government. The views and conclusions contained in this document are those of the authors and should not be interpreted to represent the official policies, either expressed or implied, of the U.S. Government.

R. M. Audet, E. H. Edwards, and D. A. B. Miller are with the Edward L. Ginzton Laboratory, Stanford University, Stanford, CA 94305 USA (e-mail: audet@stanford.edu; ehe@stanford.edu; dabm@stanford.edu).

P. Wahl was with the Edward L. Ginzton Laboratory, Stanford University, Stanford, CA 94305 USA. He is now with the Department of Applied Physics and Photonics, Vrije Universiteit Brussel, Brussels 1050, Belgium (e-mail: pierrewahl@gmail.com).

Color versions of one or more of the figures in this paper are available online at http://ieeexplore.ieee.org.

Digital Object Identifier 10.1109/JQE.2011.2167960

insertion loss. AFPMs based on the QCSE have the advantage that the high-speed response is typically not transit time-limited, and the device speed is thus determined primarily by the RC delay, except in the case of very high optical power levels [11]. In order to increase the modulation speed and decrease power consumption, it is therefore desirable to make the AFPM footprint as small as possible, since this will decrease the device capacitance. However, the use of a small modulator necessitates tight focusing of the incident optical beam. The significant angular divergence of such a beam can alter the reflection properties of the modulator's resonant cavity, thus decreasing the achievable extinction ratio.

Other effects can also influence the performance of small AFPMs. If light is coupled into and out of the device using an optical fiber or other mode-selective element, the divergence and distortion of the beam profile as it propagates through the modulator's resonant cavity will impact the modal overlap of the reflected beam with the incident mode, and hence the amount of collected reflected power. Additionally, fabrication issues, such as roughness in the various layers of the modulator structure, may also degrade the performance. Furthermore, the performance of the modulator is sensitive to optical misalignments. In this paper, we examine the relative importance of the above-mentioned effects, and, based on these results, consider the suitability of AFPMs for high-speed, low-power inter- and intra-chip optical links. This work complements previous studies of III–V AFPMs that have investigated other design considerations, such as tolerances to grown layer thickness variations and temperature fluctuations [10], [13].

B. Organization

In Section II, we review the AFPM concept and relevant performance metrics. We present a reference design of a Ge/GeSi QCSE AFPM that is used for all simulations in this paper. In Section III, we consider modulators in which the device footprint is several times the incident spot size. We examine how the reflection spectra and spatial beam profiles are altered as the incident spot size is decreased, and we consider the effects of interfacial roughness in the epitaxy and DBR mirrors.

In Section IV, we examine the performance of small micropillar modulators in which the device diameter is comparable to the spot size of a tightly-focused incident beam, such that the micropillar also functions as a vertical waveguide. We examine how the optical performance of these modulators is affected as the device size is decreased, and consider the tolerance to beam misalignment. In Section V, we propose both conservative and aggressive designs that we argue should be able to meet performance targets for practical optical interconnects. We then discuss the ultimate scaling limits for such AFP micropillar modulators.

II. Asymmetric Fabry-Perot Modulators

A. Concept

The asymmetric Fabry-Perot modulator, shown in Fig. 1, consists of two mirrors surrounding a region in which the absorption can be altered by application of an electric field.

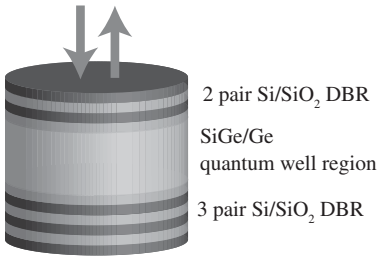

Fig. 1. Schematic illustration of a cylindrical micropillar asymmetric Fabry-Perot modulator. Light (depicted by the arrows) enters from the top. A voltage is applied across a p-i-n junction containing the active region. Field-dependent absorption in the quantum wells modulates the intensity of the reflected light.

For normal incidence, the fraction of reflected optical power on resonance, R_T, can be expressed as

$$R_T = \frac{\left|\sqrt{R_f} - \sqrt{R_{b,\text{eff}}}\right|^2}{\left|1 - \sqrt{R_f R_{b,\text{eff}}}\right|^2}, \tag{1}$$

where R_f is the front mirror reflectance, and the effective back mirror reflectance $R_{b,\text{eff}}$ is given by $R_{b,\text{eff}} = R_b \exp(-2\alpha L)$ [10]. Here, R_b is the reflectance of the back mirror (ideally near unity), α is the effective power absorption coefficient inside the cavity, and L is the cavity length. Changing α and hence $R_{b,\text{eff}}$ will alter R_T. A critically coupled condition with zero reflectance is achieved when $R_{b,\text{eff}} = R_f$, or, equivalently, when the effective absorption is $\alpha = \ln\left(R_b/R_f\right)/(2L)$.

The extinction ratio of the modulator, in decibels, is $ER = 10\log\left(R_{T,\text{on}}/R_{T,\text{off}}\right)$, where $R_{T,\text{on}}$ is the reflectance in the low absorption, high reflectance state, and $R_{T,\text{off}}$ is the reflectance in the high absorption, low reflectance state. If the critical coupling condition, $R_{T,\text{off}} \approx 0$, is reached in the high absorption state, the extinction ratio can thus approach infinity. For interconnect applications, an extinction ratio of > 7 dB is preferred, although 4–5 dB may be sufficient [1].

In addition to the contrast ratio, two other important figures of merit for the modulator are the insertion loss, $IL = 1 - R_{T,\text{on}}$, and the achievable absolute change in reflectance, $\Delta R = R_{T,\text{on}} - R_{T,\text{off}}$.

B. Simulated Structure

The structure simulated in this paper is similar to the device reported in Edwards et al. [20]. It is designed for operation near $\lambda = 1.5\,\mu$m, and is illustrated in Fig. 1. The AFP resonant cavity has $Q \approx 300$ in the high absorption state and $Q \approx 450$ in the low absorption state. Light enters perpendicular to the surface and is partially reflected off the front mirror, which is a distributed Bragg reflector (DBR) consisting of two pairs of α-Si:H/SiO_2 layers. The top Si layer of the DBR is 40 nm thick, while the other layer thicknesses are all equal to $\lambda/4$ in the respective materials. The top layer thickness was chosen such that the front mirror has an overall reflectance of 95% at normal incidence. The back mirror is a three-pair α-Si:H/SiO_2 DBR stack with $R > 99.7\%$. The high index-contrast DBRs yield high reflectances with relatively few layer pairs, using standard CMOS-compatible materials.

Similar high index-contrast DBRs have been employed as both top and bottom reflectors for vertical cavity surface emitting lasers [21], [22], microcavity light emitting diodes [23], and as the front mirror on AFPMs [24].

Light transmitted through the front mirror resonates in the 720 nm thick GeSi p-i-n structure and is partially absorbed by 15 $Ge/Ge_{0.85}Si_{0.15}$ quantum wells in the intrinsic region. For convenience, the entire GeSi active region is modeled as a homogeneous layer with wavelength-dependent absorption fit to experimental data in the range of interest. The electroabsorption parameters used in the simulation assume a 3:1 on/off absorption contrast and a background absorption in the low absorption state of 0.9% per single pass (0.06% absorption probability per quantum well) at the wavelength of interest, where the background absorption is due primarily to the indirect bandgap of germanium at $\lambda = 1.85\ \mu$m (0.67 eV). Additional loss due to scattering from interfacial roughness is considered in Section III-E, but is assumed zero elsewhere.

III. Spot Size Effects for Large Devices

Using the model structure described above, we first consider how the optical performance of large AFPMs depends on the spot size of the incident beam. In particular, we consider the case where the modulator footprint is significantly bigger than the spot size.

A. Modified Transfer Matrix Method

Reflection spectra of AFPMs are typically calculated using the 1-D transfer matrix method (TMM) [25]. However, this simple method is accurate only when the incident beam is large and the wavefronts resemble plane waves. To properly simulate device behavior with tightly focused beams, we extend the transfer matrix approach by performing a Fourier decomposition of a Gaussian beam into a weighted sum of plane waves with various spatial frequency components, then propagating each of these plane waves through the structure using the 1-D TMM, coherently adding the output plane waves to get the final output beam. This technique has previously been applied to microcavity two photon absorption photodetectors [26] and dielectric multilayer filters [27]–[29]. This section expands upon results we have previously presented for AFPMs [30]–[32].

In the large device size limit, we simulate the structure described in Section II-B by assuming it has infinite extent in the transverse plane. The reflection coefficient is calculated for plane waves incident at a variety of angles. To calculate the total reflected power, the reflection coefficients are weighted by the fraction of power in the beam incident at each angle, so the overall power reflection coefficient R is

$$R = \frac{\int_0^\infty k_x |r(k_x) E_0(k_x)|^2 \, \mathrm{d}k_x}{\int_0^\infty k_x |E_0(k_x)|^2 \, \mathrm{d}k_x} \tag{2}$$

where $E_0(k_x)$ is the amplitude of the plane wave field component with incident transverse wavevector k_x, and $r(k_x)$ is the field reflection coefficient determined by the 1-D TMM.

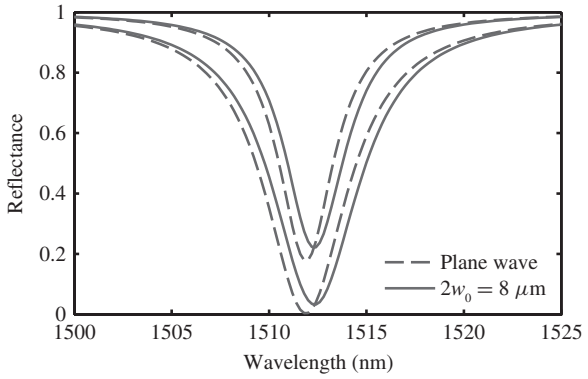

Fig. 2. Simulated reflection spectra for the high reflectance "on" and low reflectance "off" states of the AFPM for a plane wave ($w_0 = \infty$) and a Gaussian beam with spot size $2w_0 = 8\ \mu$m, showing degradation of the extinction ratio due to the finite beam size.

We note that the scaling employed in (2) effectively simulates incident beams with either azimuthal or radial polarization, and it is not strictly correct for the more common linearly or circularly polarized light beams. This is not a concern, however, when the input beam is at normal incidence and the spread in incident angles is small, since for near-normal incidence there is little polarization sensitivity. Even for relatively tightly focused beams (beam waist diameter $2w_0$ of a few microns, for $\lambda = 1.5\ \mu$m light), the majority of the angular components in the beam are at small angles of incidence. In practice, the polarization dependence of reflectances is less than 10% for a Gaussian beam with 4 μm waist diameter at normal incidence. The difference in reflection spectra quicky approaches zero for larger spot sizes.

B. Results–Spot Size Dependence

Using the approach described above, we examine the simulated reflection spectra of the modulator for different incident beam sizes. Figure 2 compares the behavior of the modulator for an incident plane wave and for a Gaussian beam with waist diameter $2w_0 = 8\ \mu$m. For the plane wave ($w_0 \to \infty$), the contrast ratio approaches infinity, since the off-state reflectance approaches zero. However, for the beam with 8 μm spot size, the off-state resonance is redshifted by 0.5 nm and the off-state reflectance at resonance (ideally zero) is 3.3%. The nonzero off-state reflectance for the Gaussian beam occurs because the AFP zero-reflectance condition can hold only for a single plane-wave incident angle. Furthermore, the resonance redshifts slightly as the spot size is decreased, because components of the beam with large incident angles will traverse the active region obliquely, increasing the effective cavity length. Finally, the reflection spectrum in the low absorption (high reflection) state will also be altered as the spot size is decreased, due to the different reflectance coefficients for beam components with different incident angles.

Figure 3(a) shows off-state curves for different spot sizes. The curve for a beam with 12 μm waist diameter is nearly identical to the ideal plane wave case. A small change is observed for an 8 μm spot size, while at 4 μm, the spot size effect becomes quite pronounced, with the minimum off-state reflectance increasing to 18%.

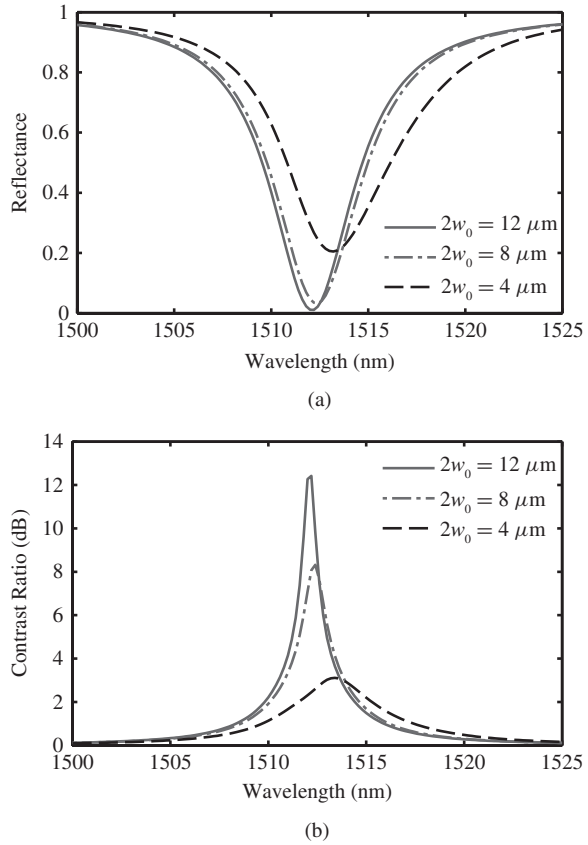

Fig. 3. (a) Calculated reflection spectra for different spot sizes. The device is simulated in the absorbing state, which yields zero reflectance on resonance for an incident plane wave (large spot size limit). (b) Plot of the modulator contrast ratio for the same spot sizes.

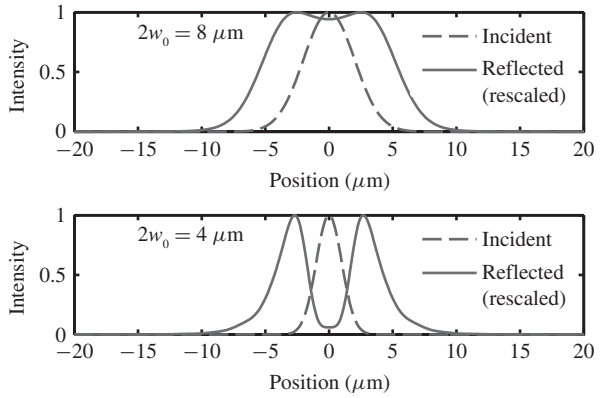

Fig. 4. Simulated transverse spatial profiles of the incident and reflected beams for two different spot sizes. The beam profiles show the squared magnitude of the electric field, and are measured 100 nm above the top surface of the resonator. The reflected intensities are rescaled for comparison purposes.

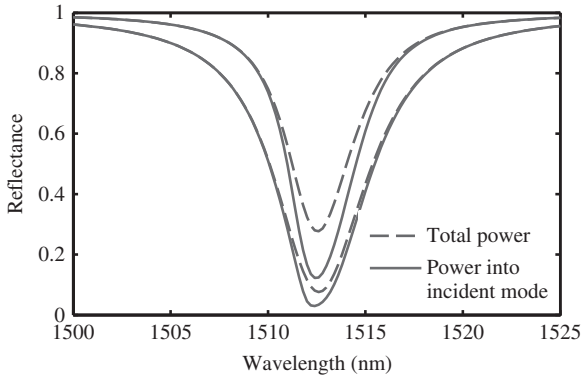

Fig. 5. Reflection spectra for a modulator in the on and off states with a 6 μm incident beam waist diameter, for total power and power coupled back into the incident Gaussian mode.

Figure 3(b) shows the associated modulator contrast ratio for different spot sizes. For the 8 μm spot, the maximum contrast ratio is 8.2 dB, compared to more than 12 dB for a 12 μm spot. For the 4 μm spot, the contrast ratio falls to 3.1 dB, which is likely unsuitable for optical interconnect applications.

The absolute change in reflectance ΔR may not be as severely affected by the spot size as the contrast ratio, however. As seen in Fig. 2, for a plane wave, the absolute reflectance change is $\Delta R = 17.3\%$, while for the Gaussian beam with an 8 μm spot, the change in reflectance is actually slightly higher, $\Delta R = 18.4\%$.

It should be noted that the large absorption contrast attainable in germanium quantum wells means that the Q factor of our resonant cavity could be chosen to be relatively low. If the absorption contrast were smaller, a higher-Q structure could be necessary to attain the desired extinction ratio. This would result in significantly worse spot size dependence, in addition to decreasing the operating bandwidth and increasing insertion loss.

C. Beam Profile and Mode Overlap Integral

The spatial profile of the reflected beam is also of interest because the reflected light may be propagated through various optical components or coupled back into an optical fiber. Figure 4 plots the incident and reflected field profiles just above the top surface of the device. For a beam focused on the top surface of the modulator, with an 8 μm spot size, the reflected beam still somewhat resembles a Gaussian, although it has broadened during propagation through the resonator. As the spot size is decreased to 4 μm, the reflected beam shape is significantly altered. This is due to the differing reflection coefficients of the various angular components.

The fraction of reflected power overlapping the original mode is given by the square of the parameter

$$\eta = \frac{\left|\iint E_i^*(x,y)E_r(x,y)\,dx\,dy\right|}{\left[\iint |E_i(x,y)|^2\,dx\,dy \iint |E_r(x,y)|^2\,dx\,dy\right]^{\frac{1}{2}}} \tag{3}$$

where E_i and E_r are the incident and reflected field amplitudes, respectively. If the system is configured such that only light coupled back into the original mode is collected, the measured reflectance spectrum will be the overlap parameter $\eta^2(\omega)$ multiplied by the fraction of total power reflected at each wavelength. Figure 5 shows the effect of including mode overlap in the reflection calculation. For a 6 μm spot, the total reflected power in the on and off states is 27.3% and 7.6%, respectively, whereas the fraction of power coupled back into the original Gaussian mode is 12.0% and 3.1%. The reflection at resonance is hence significantly lower in both the on and off states when the overlap factor η^2 is accounted for.

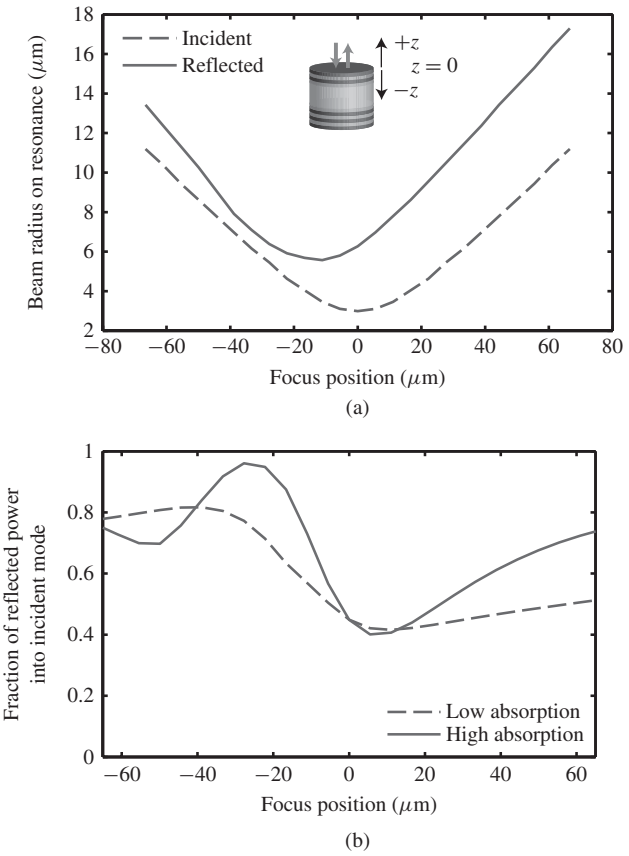

Fig. 6. Effects of the focal position, for a spot size of $2w_0 = 6\ \mu$m. (a) Plot of incident and reflected beam width for a modulator in the low reflection state, measured 100 nm above the device surface, as a function of the z-position of the focus. A value $z < 0$ corresponds to the focus located below the device surface. The beam width is defined as the radius containing 86% of the beam power. (b) Fraction of the reflected power in the incident mode, given by the squared mode overlap η^2, taken 100 nm above the device surface, in low and high absorption states, as a function of focal position.

Despite the extra insertion loss, the contrast ratio has increased from 5.6 dB to 5.9 dB, because the beam shape, and hence the overlap integral, is most dramatically altered in the low reflectance state.

D. Location of Focus

For the case of a device much larger than the incident beam, the focal position will have no effect on the reflection spectrum for the total reflected power, since the distribution of power among the various plane-wave components is not affected by the position of the focus. However, in considering the spatial profile of the reflected beam, and, in particular, the overlap integral between the incident and reflected beams, the position of the focus becomes important. Because the beam will diverge as it propagates through the resonator, to achieve maximal overlap between the incident and reflected beams just above the modulator surface, it is desirable to focus the incident beam such that the waist is located some distance into the device. By examining the incident and reflected beam widths, as shown in Fig. 6(a) for a 6 μm beam waist, we see that the reflected beam width on resonance is minimized when the focus is located approximately 15 μm below the top mirror surface.

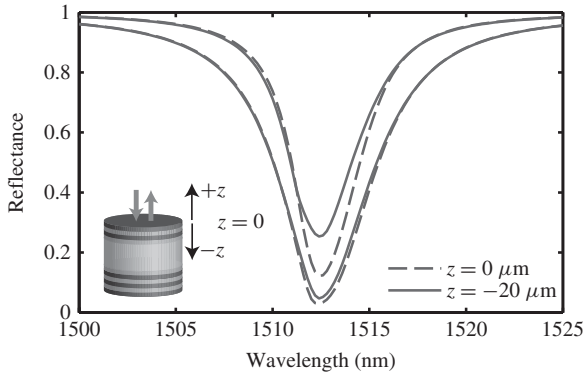

Fig. 7. Reflection spectra including modal overlap for a modulator in the on and off states, for two different focus locations: beam waist at the top surface of the modulator ($z = 0$), and beam waist displaced $-20\ \mu$m in the z direction. Simulations assume a Gaussian beam with spot size $2w_0 = 6\ \mu$m.

The reflected beam width is closely related to the fraction of power overlapping the incident mode, given by the squared mode overlap integral η^2, which is shown in Fig. 6(b). From this plot it is apparent that shifting the focus position to 20 μm beneath the top mirror surface will decrease the insertion loss when considering power coupled back into the incident mode, because there is higher mode overlap with the reflected beam in the modulator's on state at this focal position.

Figure 7 shows the effect of the focus position on the overall modulator performance when the mode overlap is considered. If the focus is chosen correctly, the insertion loss is improved. By displacing the beam waist 20 μm towards the back of the modulator (as shown in Fig. 6(a) to yield near the minimum reflected beam width), we achieve on and off state reflectances at resonance of 25% and 4.8%, respectively, and thus a contrast ratio of 7.2 dB. This compares to 12.0% and 3.1% on and off state reflectances, for 5.9 dB contrast ratio, when the beam waist is at $z = 0$.

To summarize, we have found that, for large devices, tight focusing of the incident beam can significantly decrease the extinction ratio. Taking into account the overlap of the incident and reflected beams (relevant when coupling reflected light into a fiber, for example) can increase the extinction ratio, but there is an insertion loss penalty. The correct choice of focus position can help minimize the insertion loss penalty and also improve the contrast ratio.

E. Surface Roughness

Another factor that can significantly influence the device performance is microscopic surface roughness at the various layer interfaces in the structure. The effects of surface roughness have been previously considered in a fiber-coupled AFPM design [33], as well as for a high-finesse DBR microcavity structure [34]. In both cases, it was found that the effect of interfacial roughness was small. This was due to the low-Q cavity of the AFPM and the low index contrast of the DBR mirrors in the high-finesse cavity, respectively. The present modulator design has a moderate-Q cavity and high index contrast DBRs, and thus further investigation is merited.

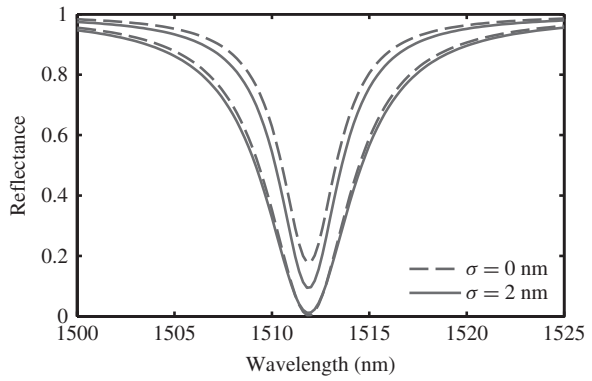

Fig. 8. Simulated modulator performance showing the effect of surface roughness at the layer interfaces. Reflection spectra are shown for the high reflectance "on" and low reflectance "off" states for a device with smooth layer interfaces and a device with Gaussian-distributed roughness with RMS value $\sigma = 2$ nm at each interface.

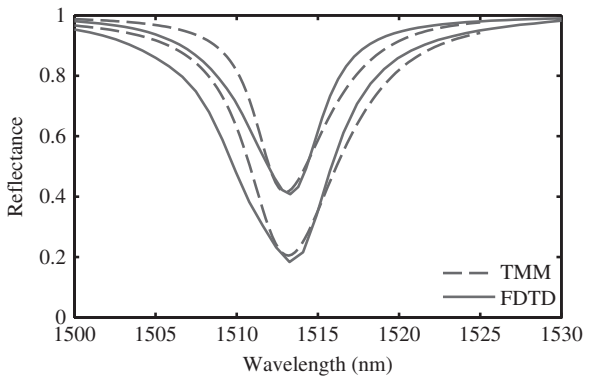

Fig. 10. Simulated modulator performance, showing high and low reflectance states in the large device size limit. The beam, with waist diameter $2\omega_0 = 4\ \mu$m, is incident upon a device with diameter $d = 20\ \mu$m (FDTD), and $d = \infty$ (TMM). Good agreement is found between the 3-D FDTD simulation and the modified TMM in this limit, especially near the resonant wavelength.

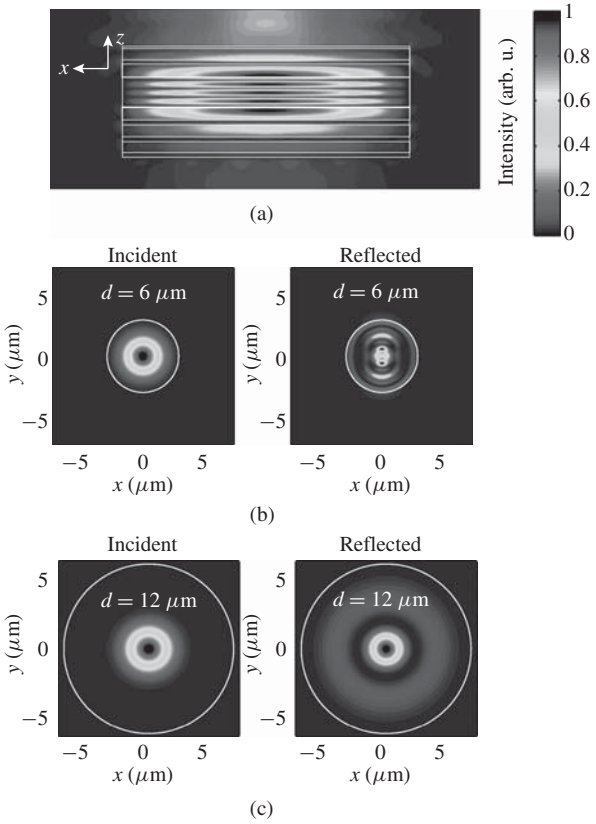

Fig. 9. Intensity profiles of the electric field, given an incident Gaussian beam with 4 μm spot size. (a) Cross-section of the modulator, on resonance in the low reflection state. The beam is incident from the top onto the modulator with pillar diameter of $d = 6\ \mu$m. The layer interfaces are indicated in white. (b) Plot of incident and reflected beam profiles, for a modulator pillar diameter $d = 6\ \mu$m, taken 100 nm above the modulator surface, with reflected intensities rescaled for clarity. (c) Incident and reflected beams, for modulator with pillar diameter $d = 12\ \mu$m.

We model the effects of surface roughness by incorporating scattering loss into our transfer matrix simulation. For a material with small Gaussian-distributed thickness variations with RMS value σ, where $\sigma/\lambda \ll 1$, we can modify the Fresnel coefficients, as in Eq. 9 of Mitsas et al. [25] to take into account the scattering loss that modifies the amount of specular reflection and refraction [35]–[38].

We assume for simplicity that every interface in the structure has independent Gaussian-distributed roughness with RMS value $\sigma = 2$ nm, towards the upper limit of what would be expected on a fabricated device. We simulate a plane wave at normal incidence. The calculated performance of the modulator for identical absorption parameters with and without surface roughness is presented in Fig. 8. The on/off state reflectances change from 17.3% and 0% for the ideal case to 9.0% and 1.2% (8.7 dB extinction ratio) when surface roughness is considered. The main effect is thus a substantial decrease in the on state reflectance, meaning higher insertion loss and lower absolute change in reflectance between the on and off states. The change in the off state reflectance is relatively unimportant. Because losses due to non-specular reflection from surface roughness are indistinguishable from absorption losses inside the cavity, it is still possible to achieve the zero reflectance condition even with surface roughness; however, the amount of absorption necessary in the cavity to reach critical coupling is altered due to the presence of surface roughness as an additional loss mechanism.

In the modified Fresnel coefficients [25], the scattering loss due to surface roughness is proportional to the difference between the refractive indices at each interface. In this regard, the present design with high index contrast mirrors is particularly sensitive to interfacial roughness. The effects of surface roughness could potentially be decreased by switching to lower-contrast DBR materials, such as Si_3N_4/SiO_2, at some cost of reduced operating bandwidth because of the deeper penetration into the lower index-contrast mirrors.

IV. FDTD Simulations of Small-Diameter Devices

A. Method

While the modified transfer matrix method results above give insight into the behavior of devices for which the modulator dimensions are significantly larger than the spot size, the usual one-dimensional TMM cannot account for optical confinement in the transverse directions. To model small

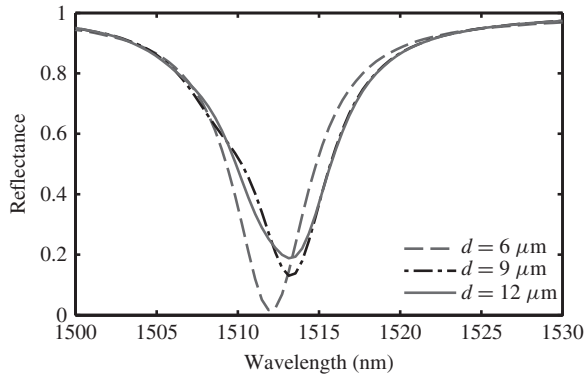

Fig. 11. 3-D FDTD simulations of reflectance spectra for three devices with different pillar diameters, d, operating in the off (low reflectance) state, for a tightly focused beam with spot size $2w_0 = 4\ \mu$m. The minimum reflectance is improved by decreasing the modulator size to better match the incident spot size.

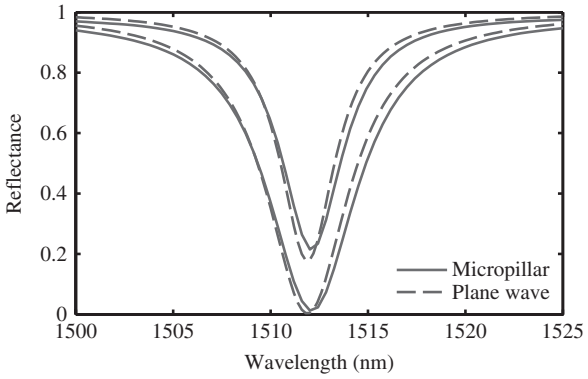

Fig. 12. Spectra for a modulator with pillar diameter $d = 6\ \mu$m, for an incident Gaussian beam with spot size $2w_0 = 4\ \mu$m, simulated by 3-D FDTD, plotted against spectra for a modulator with infinite transverse extent and an incident plane wave, simulated by TMM. The close agreement between the two sets of curves illustrates that near-ideal performance can be achieved when the pillar diameter is well-matched to the incident spot size.

modulators in which the device diameter is comparable to the spot size of the incident beam, we perform finite-difference time-domain (FDTD) simulations [39], and examine how the optical performance of the modulators is affected as the device size is decreased. We find that in small "micropillar" devices, vertical (i.e., surface-normal) waveguiding effects can act in a manner that substantially benefit device performance.

We perform both 2-D and 3-D FDTD simulations of the modulator described in Section II-B. In contrast to the structure simulated with the TMM, which had infinite extent in the xy plane, the device here is a cylindrical pillar and thus light is confined in the transverse directions. The incident Gaussian beam is TE-polarized and focused on the top surface of the modulator for all the FDTD simulations presented here. The simulations are performed using custom FDTD code running on an NVIDIA graphics processing unit (GPU) [40].

B. Results

Figure 9(a) shows a cross-sectional view of the simulated optical electric field intensity within a modulator on resonance in the low reflectance state. We note the strong enhancement of the field inside the resonant cavity. Also apparent is the relatively short propagation length of the electric field into the high index-contrast DBR mirrors. Figures 9(b) and (c) show the incident and reflected beam profiles for different device sizes. In Fig. 10, good agreement is observed between the Gaussian beam TMM simulations and 3-D FDTD for a spot size of 4 μm, in the limiting case of a structure with large dimensions ($d = 20\ \mu$m for FDTD, infinite for TMM). We note that for this large device, the minimum reflectance is 18% for the low reflection state, thus limiting the contrast ratio to 3.3 dB. The same layer structure illuminated by a plane wave would exhibit zero reflectance in the off state.

Figure 11 shows that the minimum reflectance for the same spot size can be significantly lower than the 18% quoted above if the modulator pillar diameter is chosen appropriately. As the diameter is decreased, the reflectance falls from 18% for a 12 μm pillar to a minimum of approximately 1% for a 6 μm pillar.

Figure 12 compares the performance of the modulator with a 6 μm pillar diameter and 4 μm beam waist to the TMM result for a semi-infinite modulator with an incident plane wave. The FDTD results show a contrast ratio of 12.3 dB and an absolute reflectance change of $\Delta R = 20.2\%$. This performance is very close to the ideal plane wave scenario, which has a large extinction ratio and $\Delta R = 17.3\%$. Hence, it appears that good optical performance can be achieved even from small diameter AFPM structures when the pillar size is chosen appropriately.

C. Optimal Pillar Size

A series of 2-D FDTD simulations was performed to better understand how varying the micropillar size affects the reflection spectra. The minimum device reflectance in the absorbing state was calculated as a function of both the incident beam size $2w_0$ and the pillar diameter d. The results are shown in Fig. 13(a). A linear relationship exists between the beam waist and the pillar diameter yielding minimum reflectance, with the optimum from these numerical simulations occuring for $2w_0/d \approx 0.7$.

This linear trend can be understood intuitively in terms of the coupling efficiency between the incident beam and a high-index cylindrical dielectric waveguide. Figure 13(b) shows the calculated overlap integral between a Gaussian beam and the fundamental mode of a GeSi cylinder, which is maximized for nearly the same ratio of beam size to pillar diameter $2w_0/d = 0.7$ as was found optimal for the modulators in Fig. 13(a). The maximum squared mode overlap integral $\eta^2 > 99\%$ indicates excellent mode matching between the incident Gaussian beam and the cylindrical waveguide mode. As such, in the off state at resonance, the incident beam experiences near perfect coupling into the AFPM. Furthermore, when the bias is set appropriately, all light coupled into the modulator will be completely absorbed. Thus, it is possible to achieve near zero reflectance with an appropriately sized micropillar modulator.

The above mode matching argument is somewhat simplistic, as the modulator is not homogenous in the z direction.

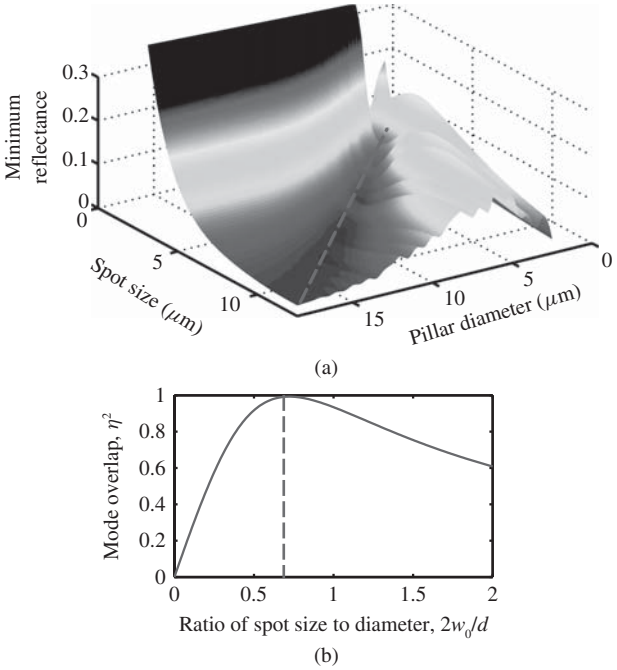

Fig. 13. (a) Scaled 2-D FDTD results, showing the minimum reflectance in the off state of the modulator as a function of beam waist $2w_0$ and pillar diameter d. The dotted red line denotes the points with $2w_0/d = 0.7$. (b) Calculated squared mode overlap integral between a Gaussian beam with spot size $2w_0$ and the fundamental mode of a GeSi cylinder with diameter d, as a function of the ratio $2w_0/d$. The maximum overlap occurs for $2w_0/d \approx 0.7$.

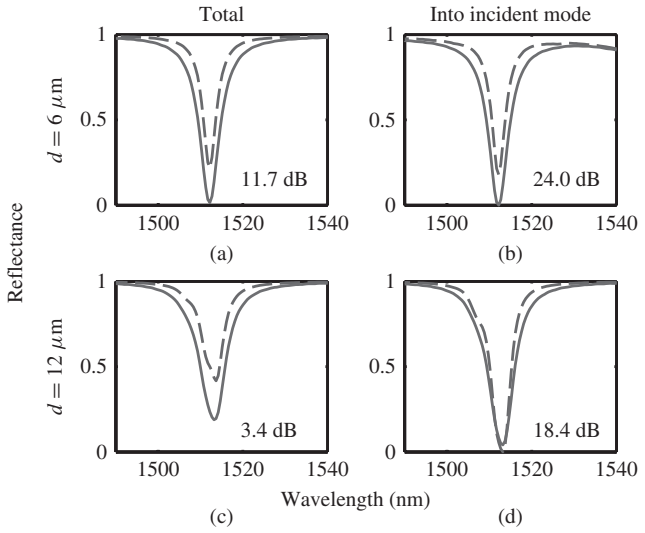

Fig. 14. Effect of mode overlap, for an incident beam with waist diameter $2w_0 = 4\ \mu$m. Reflection spectra are plotted for modulators in the nominally low (red, solid curve) and nominally high (blue, dashed curve) reflectance states. Plot (a) shows the reflection spectrum for the total reflected power, while plot (b) shows the power coupled back into the incident mode, calculated for a pillar with diameter $d = 6\ \mu$m. Plots (c) and (d) show the same for a pillar with diameter $d = 12\ \mu$m. The extinction ratio on resonance is noted on each plot.

However, both the SiO_2 and the semiconductor material have sufficiently high index contrast with the surrounding air such that the field remains confined and the transverse profile of the fundamental mode is similar throughout the structure. Hence, considering the optimal modulator sizing from the perspective of this simple mode overlap argument is quite instructive.

D. Mode Overlap Integral

As was done in the case of large devices using TMM simulations, we now consider how the reflection spectra for small modulators are altered when the reflected beams are coupled into an optical fiber or other mode-selective element. Here, 3-D FDTD simulations were used to solve for the fields.

Figure 14 shows the effect of including the fraction of power coupled back into the original mode in the reflection calculation. First, we compare parts (a) and (b), which show spectra for a device in which the pillar diameter is optimally matched to the incident beam spot size. There is little difference between (a), which shows the total reflected power, and (b), which shows the fraction of power reflected back into the incident mode, because the waveguiding effect of the pillar minimizes the spatial redistribution of the beam as it propagates through the resonator. Off resonance, the mode overlap integral (3) is nearly unity. At resonance, in the high reflectance state, the mode field overlap integral is still above 90%.

In contrast, in Fig. 14(c) and (d), we see that modal overlap has a significant effect when the pillar is larger than optimal for the given spot size. For the 4 μm spot, with a pillar diameter of 12 μm (compared to the optimal diameter of 6 μm), we see a substantial decrease in reflectance of the high reflectance state when the modal overlap is considered, from 17.89% in Fig. 14(b) for the 6 μm pillar to 0.06% in Fig. 14(d) for the 12 μm pillar. In fact, the reflectance in the low absorption (nominal high reflectance) state is actually lower than in the high absorption (nominal low reflectance) state, resulting in a transition from a normally-on to a normally-off device, as well as large insertion loss, although the predicted extinction ratio remains relatively high.

We note here that the above simulations were performed with the focus position on top of the front mirror, which is the optimal position when the modulator when pillar is sized correctly. For modulators where the pillar is too large relative to the incident beam, the same effects described in III-D will be observed, with the optimum focus point being towards the bottom of the device.

E. Misalignment Tolerance

The results presented previously have all assumed that the incident beam is perfectly centered on the surface of the modulator. However, any practical system involving dense arrays of thousands of modulators will need to maintain a degree of tolerance to beam misalignment. FDTD simulations were performed to analyze the impact of varying amounts of misalignment on the performance of the modulators.

Figure 15 shows spectra in the on and off state for a device with a 6 μm pillar diameter, when the incident beam with 4 μm spot size has a lateral misalignment of $\Delta x = 0$, 0.5, and 1 μm. The extinction ratios in the three cases are 11.9 dB, 7.4 dB, and 4.0 dB, respectively. To maintain a target 7 dB extinction ratio over at least 1 nm bandwidth, a lateral

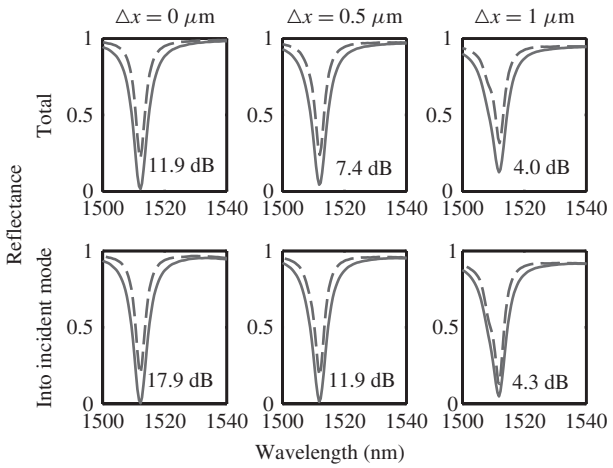

Fig. 15. Effect of different values of beam misalignment on the modulator performance, for a modulator with diameter $d = 6\ \mu$m and a spot size of $4\ \mu$m, for total reflected power (top), and reflected power coupled back into the incident mode (bottom). The extinction ratio on resonance is noted on each plot.

misalignment of $\Delta x < \pm 0.5\ \mu$m is acceptable. It is possible to increase the pillar diameter somewhat to try to improve the alignment tolerance, but if the spot size is kept the same, the loss of waveguiding due to the larger pillar can lessen the degree of improvement that would otherwise be seen. As an example, for the same spot size but a larger device diameter of 7 μm, the extinction ratios for $\Delta x = 0$, 0.5, and 1 μm are 8.0 dB, 6.38 dB, and 4.8 dB, respectively.

The bottom panel of Fig. 15 shows power coupled back into the original mode for a 4 μm spot incident upon the 6 μm diameter micropillar modulator. We again observe that the extinction ratio degrades as the misalignment increases. Overall, the extinction ratio is higher in the case where mode overlap is considered, at the expense of greater insertion loss.

The modulator performance will also be degraded if the incident beam is not perfectly perpendicular to the device surface. An FDTD simulation was performed to examine the tolerance to such angular misalignments. For the device with a 6 μm pillar diameter and an incident beam with 4 μm waist, assuming no lateral misalignment, the angular misalignment $\Delta\theta$ must be less than ± 3 degrees to maintain at least 7 dB extinction ratio over 1 nm bandwidth.

V. Proposed Designs

For optical interconnects to be a compelling replacement for electrical links, we need to target device energies in a 10-year timescale of 10–50 fJ/bit for off-chip and 2–10 fJ/bit for on-chip interconnects, respectively [5]. Given a desired extinction ratio of 7 dB, and the modulator structure considered throughout this paper, we now propose three sets of specific device dimensions. The proposed designs are shown in Table I. The table specifies the pillar diameter and spot size, as well as the extinction ratio (ignoring mode overlap), alignment tolerance, and switching energy associated with each design.

For the proposed designs, the modulator's switching energy per bit was taken to be $E = CV^2$, assuming a 1 V drive voltage. Such an energy definition includes the energy stored in the capacitor after it is charged and the energy necessarily dissipated in the resistance of the driver circuit during charging, and presumes this energy is dissipated for every bit. If we presume non-return-to-zero signaling, in which on average the voltage on the capacitor is only changed every other bit, the energy per bit would be half of our quoted numbers. It would also be possible to presume that when transitioning from a charged state to a discharged state, which on the average will happen every other bit transition, there is no additional power drawn from the power supply because we are merely discharging the capacitor, then we could divide our average energy per bit by another factor of 2. Here we take the most conservative approach to this energy, however, noting that we have also not included possible energy dissipation due to photocurrent, a dissipation that could be comparable to the capacitive energy dissipation [41]. The device capacitance C (ignoring parasitics) was approximated by the parallel plate capacitance $C = \epsilon A / x_d$, where ϵ is the dielectric constant, A is the device area, and x_d is the thickness of the depletion layer within the p-i-n active region, which for the simulated device is approximately 350 nm.

TABLE I
Proposed Device Designs

Design	Pillar (μm)	Spot (μm)	ER (dB)	Align. Tol. ($\pm\mu$m)	Energy (fJ/bit)
No waveguiding	>12	8	8	As desired	>45
Conservative	8.5	6	13	0.75	20
Aggressive	6	4	12	0.5	10

The first design, labeled "no waveguiding" in Table I, utilizes a large spot size of 8 μm, so that beam diffraction during propagation through the resonator is minimal. This design is the most conservative of the three, because the performance is not substantially dependent on the pillar size, as long as the pillar is large enough to contain the entire incident spot. Hence, the lateral alignment tolerance can be made arbitrarily large by simply increasing the pillar size. The large spot size, and hence large pillar diameter means that the device energy per bit will be higher than the other two designs, which rely upon waveguiding to achieve good extinction ratios with smaller pillars. However, the minimum energy consumption of 45 fJ/bit for the smallest version of this no-waveguiding design still places it within the range of target device energies for off chip links [5], so a device of such dimensions could indeed be useful.

The next design, which we consider a conservative approach, achieves good contrast ratios with a smaller pillar diameter and spot size due to waveguiding by the pillar. The incident spot size of 6 μm requires a pillar diameter of approximately 8.5 μm to achieve optimal performance. The projected energy consumption of the conservative design, 20 fJ/bit, would make it very attractive for chip-to-chip interconnects.

Simulations show an alignment tolerance for the conservative design of $\Delta x = \pm 0.75\ \mu$m, over which a contrast ratio over 7 dB is maintained with 1 nm bandwidth. Although this tolerance is quite tight, the question of alignment tolerance in highly parallel free space links has been considered in

depth elsewhere [42], [43]. A variety of schemes have been developed to facilitate alignment and packaging of massively parallel links [44], [45]. The use, for example, of lithographically defined micro-lenses could enable such beam alignment tolerances to be achieved across all devices on the chip.

Our aggressive design relies upon a smaller spot size of 4 μm, and exhibits tighter alignment tolerance of $\Delta x = \pm 0.5$ μm to maintain a 7 dB contrast ratio over 1 nm bandwidth. The low energy consumption of 10 fJ/bit opens up the possibility of using it for intra-chip as well as inter-chip connections.

The small capacitances of both the conservative and aggressive designs should allow high-speed modulation at tens of GHz, assuming low resistance contacts to the germanium p-i-n structure can be achieved. There are, however, some challenges in electrically contacting the micropillar modulators. While techniques are available to improve the resistance of metal contacts to germanium [46], as device size is decreased to minimize capacitance, the contact resistance will increase due to the smaller contact area. Since the modulation rate of QCSE AFPMs is limited primarily by the RC delay, for high-speed operation the contact resistance may restrict the minimum feasible device size. Furthermore, for the devices requiring waveguiding (spot sizes less than 8 μm), it is important that the contacts be placed such that the interaction between the contacts and the optical mode is minimized, and, simultaneously, such that the correct pillar diameter is maintained, in order to minimize diffractive effects. Similar contact difficulties have been successfully addressed in micropillar lasers using lateral contacting, with the contact pads resting on top of an insulating polymer surrounding the pillars [47]. This leaves the top of the micropillars free of metal, so that the optical properties are minimally impacted.

While the aggressive design is already projected to operate at energy levels that could be usable for on-chip links, it is worth considering what the ultimate limit of the micropillar modulator size may be. As was suggested in section IV-C, the modulator design should provide good contrast ratios so long as the incident beam profile can be well matched to the fundamental mode of the micropillar. This implies that the minimum size would be set by the ability to form precisely aligned, diffraction-limited spots on the modulator surface. Reductions in diameter down to approximately half a wavelength are possible in principle, which leaves open the possibility of up to about one order of magnitude further reduction in energy, though such device structures would be very challenging to fabricate, contact, and align.

VI. Conclusion

As device size plays a key role in determining the energy consumption of AFPMs, this work has identified size-dependent factors that influence the minimum feasible modulator dimensions. To do this, we have considered the design of a realistic AFPM based on the QCSE in Ge/SiGe quantum wells, as this material system is compatible with CMOS processes and hence attractive for optical interconnect applications. For small devices, it was shown that diffraction effects may significantly degrade device performance unless the modulator pillar diameter is matched to the spot size of the incident beam. Alignment tolerances and other nonidealities were also considered.

Based on our investigations, we have presented three device designs maintaining > 7 dB extinction ratio with device energies as low as 10 fF/bit. This suggests that asymmetric Fabry-Perot electroabsorption modulators in CMOS-compatible material systems could enable efficient free-space optical connections in and out of the surface of silicon chips, providing the interconnect density and bandwidth necessary to meet the needs of future computing systems.

References

[1] G. T. Reed, G. Mashanovich, F. Y. Gardes, and D. J. Thomson, "Silicon optical modulators," *Nature Photon.*, vol. 4, no. 8, pp. 518–526, 2010.

[2] D. A. B. Miller, "Rationale and challenges for optical interconnects to electronic chips," *Proc. IEEE*, vol. 88, no. 6, pp. 728–749, Jun. 2000.

[3] A. V. Krishnamoorthy, R. Ho, X. Zheng, H. Schwetman, J. Lexau, P. Koka, G. Li, I. Shubin, and J. E. Cunningham, "Computer systems based on silicon photonic interconnects," *Proc. IEEE*, vol. 97, no. 7, pp. 1337–1361, Jul. 2009.

[4] S. Beamer, C. Sun, Y. Kwon, A. Joshi, C. Batten, V. Stojanovic, and K. Asanovic, "Re-architecting DRAM memory systems with monolithically integrated silicon photonics," in *Proc. 37th Annu. Int. Symp. Comput. Architect.*, Saint-Malo, France, 2010, pp. 129–140.

[5] D. A. B. Miller, "Device requirements for optical interconnects to silicon chips," *Proc. IEEE*, vol. 97, no. 7, pp. 1166–1185, Jun. 2009.

[6] A. G. Kirk, D. V. Plant, T. H. Szymanski, Z. G. Vranesic, F. A. P. Tooley, D. R. Rolston, M. H. Ayliffe, F. K. Lacroix, B. Robertson, E. Bernier, and D. F.-Brosseau, "Design and implementation of a modulator-based free-space optical backplane for multiprocessor applications," *Appl. Opt.*, vol. 42, no. 14, pp. 2465–2481, May 2003.

[7] M. Haney, M. Christensen, P. Milojkovic, G. Fokken, M. Vickberg, B. Gilbert, J. Rieve, J. Ekman, P. Chandramani, and F. Kiamilev, "Description and evaluation of the FAST-Net smart pixel-based optical interconnection prototype," *Proc. IEEE*, vol. 88, no. 6, pp. 819–828, Jun. 2000.

[8] F. B. McCormick, T. J. Cloonan, F. A. P. Tooley, A. L. Lentine, J. M. Sasian, J. L. Brubaker, R. L. Morrison, S. L. Walker, R. J. Crisci, R. A. Novotny, S. J. Hinterlong, H. S. Hinton, and E. Kerbis, "Six-stage digital free-space optical switching network using symmetric self-electro-optic-effect devices," *Appl. Opt.*, vol. 32, no. 26, pp. 5153–5171, 1993.

[9] M. Whitehead and G. Parry, "High-contrast reflection modulation at normal incidence in asymmetric multiple quantum well Fabry-Perot structure," *Electron. Lett.*, vol. 25, no. 9, pp. 566–568, Apr. 1989.

[10] R. H. Yan, R. J. Simes, and L. A. Coldren, "Surface-normal electroabsorption reflection modulators using asymmetric Fabry-Perot structures," *IEEE J. Quantum Electron.*, vol. 27, no. 7, pp. 1922–1931, Jul. 1991.

[11] C. C. Barron, C. J. Mahon, B. J. Thibeault, and L. A. Coldren, "Design, fabrication and characterization of high-speed asymmetric Fabry-Perot modulators for optical interconnect applications," *Opt. Quantum Electron.*, vol. 25, no. 12, pp. S885–S898, Dec. 1993.

[12] P. Zouganeli, P. J. Stevens, D. Atkinson, and G. Parry, "Design trade-offs and evaluation of the performance attainable by GaAs-$Al_{0:3}Ga_{0:7}As$ asymmetric Fabry-Perot modulators," *IEEE J. Quantum Electron.*, vol. 31, no. 5, pp. 927–943, May 1995.

[13] P. Zouganeli and G. Parry, "Evaluation of the tolerance of asymmetric Fabry-Perot modulators with respect to realistic operating conditions," *IEEE J. Quantum Electron.*, vol. 31, no. 6, pp. 1140–1151, Jun. 1995.

[14] D. A. B. Miller, D. S. Chemla, T. C. Damen, A. C. Gossard, W. Wiegmann, T. H. Wood, and C. A. Burrus, "Band-edge electroabsorption in quantum well structures: The quantum-confined Stark effect," *Phys. Rev. Lett.*, vol. 53, no. 22, pp. 2173–2176, Nov. 1984.

[15] Y.-H. Kuo, Y. K. Lee, Y. Ge, S. Ren, J. E. Roth, T. I. Kamins, D. A. B. Miller, and J. S. Harris, "Quantum-confined Stark effect in Ge/SiGe quantum wells on Si for optical modulators," *IEEE J. Sel. Topics Quantum Electron.*, vol. 12, no. 6, pp. 1503–1513, Nov.–Dec. 2006.

[16] S. Ren, Y. Rong, T. I. Kamins, J. S. Harris, and D. A. B. Miller, "Selective epitaxial growth of $Ge/Si_{0.15}Ge_{0.85}$ quantum wells on Si substrate using reduced pressure chemical vapor deposition," *Appl. Phys. Lett.*, vol. 98, no. 15, pp. 151108-1–151108-3, Apr. 2011.

[17] R. K. Schaevitz, J. E. Roth, S. Ren, O. Fidaner, and D. A. B. Miller, "Material properties of Si-Ge/Ge quantum wells," *IEEE J. Sel. Topics Quantum Electron.*, vol. 14, no. 4, pp. 1082–1089, Jul.–Aug. 2008.

[18] R. K. Schaevitz, E. H. Edwards, R. M. Audet, Y. Rong, S. Ren, S. A. Claussen, E. Tasyurek, J. E. Roth, J. S. Harris, and D. A. B. Miller, "Simple electroabsorption model for germanium quantum well devices," in *Proc. 10th Int. Conf. Numerical Simulat. Optoelectron. Devices*, Atlanta, GA, 2010, pp. 109–110.

[19] J. E. Roth, O. Fidaner, R. K. Schaevitz, Y. Kuo, T. I. Kamins, J. S. Harris, and D. A. B. Miller, "Optical modulator on silicon employing germanium quantum wells," *Opt. Express*, vol. 15, no. 9, pp. 5851–5859, Apr. 2007.

[20] E. H. Edwards, R. M. Audet, S. A. Claussen, R. K. Schaevitz, E. Tasyurek, S. Ren, O. I. Dosunmu, M. S. Ünlü, and D. A. B. Miller, "Si-Ge surface-normal asymmetric Fabry-Perot quantum-confined Stark effect electroabsorption modulator," in *Proc. IEEE Photonics Soc. Summer Topical Meetings*, Playa del Carmen, Mexico, 2010, pp. 211–212.

[21] H. Wada, D. Babic, D. Crawford, T. Reynolds, J. Dudley, J. Bowers, E. Hu, J. Merz, B. Miller, U. Koren, and M. Young, "Low-threshold, high-temperature pulsed operation of InGaAsP/InP vertical cavity surface emitting lasers," *IEEE Photon. Technol. Lett.*, vol. 3, no. 11, pp. 977–979, Nov. 1991.

[22] C. Levallois, A. L. Corre, S. Loualiche, O. Dehaese, H. Folliot, C. Paranthoen, F. Thoumyre, and C. Labbe, "Si wafer bonded of a-Si/a-SiN_x distributed Bragg reflectors for 1.55-μm-wavelength vertical cavity surface emitting lasers," *J. Appl. Phys.*, vol. 98, no. 4, pp. 043107-1–043107-5, Aug. 2005.

[23] J. Potfajova, B. Schmidt, M. Helm, T. Gemming, M. Benyoucef, A. Rastelli, and O. G. Schmidt, "Microcavity enhanced silicon light emitting pn-diode," *Appl. Phys. Lett.*, vol. 96, no. 15, pp. 151113-1–151113-3, Apr. 2010.

[24] S. J. B. Yoo, M. A. Koza, R. Bhat, and C. Caneau, "1.5 μm asymmetric Fabry-Perot modulators with two distinct modulation and chirp characteristics," *Appl. Phys. Lett.*, vol. 72, no. 25, pp. 3246–3248, Jan. 1998.

[25] C. L. Mitsas and D. I. Siapkas, "Generalized matrix method for analysis of coherent and incoherent reflectance and transmittance of multilayer structures with rough surfaces, interfaces, and finite substrates," *Appl. Opt.*, vol. 34, no. 10, pp. 1678–1683, Apr. 1995.

[26] J. O'Dowd, W. Guo, M. Lynch, A. Bradley, and J. Donegan, "Acceptance angle influence on the optimum incident spot size for high-finesse microcavity two-photon absorption photodetectors," *IEEE J. Quantum Electron.*, vol. 45, no. 12, pp. 1584–1589, Dec. 2009.

[27] F. Koyama, Y. Aoki, and K. Iga, "Spot size dependence of filtering characteristics in dielectric multilayer filters for WDM applications," in *Proc. Optical Interference Coatings*, Banff, Canada, 2001, p. WA5.

[28] S. Suda and F. Koyama, "Spot-size and incident angle dependence of filtering characteristics of narrow pass-band dielectric multilayer filters," *IEICE Electron. Express*, vol. 1, no. 14, pp. 442–446, 2004.

[29] S. Suda and F. Koyama, "Characterization of spot-size dependence of coarse wavelength division multiplexing dielectric multilayer thin-film filters for planner lightwave circuit platforms," *Jpn. J. Appl. Phys.*, vol. 44, no. 39, pp. L1225–L1227, 2005.

[30] N. C. Helman, J. E. Roth, D. P. Bour, H. Altug, and D. A. B. Miller, "Misalignment-tolerant surface-normal low-voltage modulator for optical interconnects," *IEEE J. Sel. Topics Quantum Electron.*, vol. 11, no. 2, pp. 338–342, Apr. 2005.

[31] J. E. Roth, "Electroabsorption modulators for CMOS compatible optical interconnects in III-V and group IV materials," Ph.D. dissertation, Dept. Elect. Eng., Stanford Univ., CA, 2007.

[32] R. M. Audet, E. H. Edwards, S. A. Claussen, S. Ren, R. K. Schaevitz, E. Tasyurek, and D. A. B. Miller, "Spot size effects in asymmetric Fabry-Perot electroabsorption modulators," in *Proc. IEEE Photonics Soci. Summer Topical Meetings*, Playa del Carmen, Mexico, 2010, pp. 225–226.

[33] M. Xu, B. Nener, and J. Dell, "Design of externally tuned asymmetric fibre Fabry-Perot electroabsorption optical modulators," *IEE Proc. Optoelectron.*, vol. 145, no. 6, pp. 344–352, Dec. 1998.

[34] R. P. Stanley, R. Houdre, U. Oesterle, M. Gailhanou, and M. Ilegems, "Ultrahigh finesse microcavity with distributed Bragg reflectors," *Appl. Phys. Lett.*, vol. 65, no. 15, pp. 1883–1885, Oct. 1994.

[35] I. Filiński, "The effects of sample imperfections on optical spectra," *Phys. Status Solidi B*, vol. 49, no. 2, pp. 577–588, Feb. 1972.

[36] J. Szczyrbowski and A. Czapla, "Optical absorption in D.C. sputtered InAs films," *Thin Solid Films*, vol. 46, no. 2, pp. 127–137, Oct. 1977.

[37] C. C. Katsidis and D. I. Siapkas, "General transfer-matrix method for optical multilayer systems with coherent, partially coherent, and incoherent interference," *Appl. Opt.*, vol. 41, no. 19, pp. 3978–3987, Jul. 2002.

[38] E. Nichelatti, M. Montecchi, and R. Montereali, "Optical reflectance and transmittance of a multilayer coating affected by refractive-index inhomogeneity, interface roughness, and thickness wedge," *J. Non-Cryst. Solids*, vol. 355, nos. 18–21, pp. 1115–1118, Jul. 2009.

[39] A. Taflove and S. C. Hagness, *Computation Electrodynamics: The Finite-Difference Time-Domain Method*, 3rd ed. Artech House, U.K., 2005, p. 58.

[40] P. Wahl, D. S. Ly-Gagnon, C. Debaes, D. A. B. Miller, and H. Thienpont, "B-CALM: An open-source GPU-based 3-D-FDTD with multi-pole dispersion for plasmonics," in *Proc. Int. Conf. Numerical Simulat. Optoelectron. Devices*, Rome, Italy, Sep. 2011, p. MB2.

[41] A. V. Krishnamoorthy and D. A. B. Miller, "Scaling optoelectronic-VLSI circuits into the 21st century: A technology roadmap," *IEEE J. Sel. Topics Quantum Electron.*, vol. 2, no. 1, pp. 55–76, Apr. 1996.

[42] A. G. Kirk, D. V. Plant, M. H. Ayliffe, M. Chateauneuf, and F. Lacroix, "Design rules for highly parallel free-space optical interconnects," *IEEE J. Sel. Topics Quantum Electron.*, vol. 9, no. 2, pp. 531–547, Mar.–Apr. 2003.

[43] H. Takahara, "Optoelectronic multichip module packaging technologies and optical input/output interface chip-level packages for the next generation of hardware systems," *IEEE J. Sel. Topics Quantum Electron.*, vol. 9, no. 2, pp. 443–451, Mar.–Apr. 2003.

[44] M. Jarczynski, T. Seiler, and J. Jahns, "Integrated 3-D optical multilayer using free-space optics," *Appl. Opt.*, vol. 45, no. 25, pp. 6335–6341, 2006.

[45] C. Debaes, M. Vervaeke, V. Baukens, H. Ottevaere, P. Vynck, P. Tuteleers, B. Volckaerts, W. Meeus, M. Brunfaut, J. Van Campenhout, A. Hermanne, and H. Thienpont, "Low-cost microoptical modules for MCM level optical interconnections," *IEEE J. Sel. Topics Quantum Electron.*, vol. 9, no. 2, pp. 518–530, Mar.–Apr. 2003.

[46] J. J. Lin, A. M. Roy, A. Nainani, Y. Sun, and K. C. Saraswat, "Increase in current density for metal contacts to n-germanium by inserting TiO_2 interfacial layer to reduce Schottky barrier height," *Appl. Phys. Lett.*, vol. 98, no. 9, pp. 092113-1–092113-3, Feb. 2011.

[47] C. Böckler, S. Reitzenstein, C. Kistner, R. Debusmann, A. Löffler, T. Kida, S. Höfling, A. Forchel, L. Grenouillet, J. Claudon, and J. M. Gérard, "Electrically driven high-Q quantum dot-micropillar cavities," *Appl. Phys. Lett.*, vol. 92, no. 9, pp. 091107-1–091107-3, Mar. 2008.

Ross M. Audet (S'11) received the A.B. degree in engineering sciences and physics from Harvard University, Cambridge, MA, in 2007, and the M.S. degree from Stanford University, Stanford, CA, in 2009. He is currently pursuing the Ph.D. degree in electrical engineering from Stanford University.

His research interests include silicon-compatible optoelectronic devices, optical interconnects, and quantum well devices.

Elizabeth H. Edwards (M'02) received the B.S. degree in electrical engineering from the University of Illinois, Chicago, in 2003, and the M.S. degree in electrical engineering from Stanford University, Stanford, CA, in 2008, where she is currently pursuing the Ph.D. degree in electrical engineering.

She joined the IBM Engineering and Technology Services Department, Rochester, MN, where she was involved in application-specific integrated circuit design for various projects including the Blue Gene P supercomputer. Her current research interests include photonic interconnects.

Pierre Wahl received the B.S. degree in electrical engineering and the Erasmus Mundus M.S. degree in photonics from Vrije Universiteit Brussel, Brussels, Belgium, in 2007 and 2010, respectively. He wrote his Masters thesis at Interuniversity Microelectronics Center, Leuven, Belgium, in 2010, on high frequency electrical voltage-controlled oscillators. He is currently pursuing the Ph.D. degree in electrical engineering from Vrije Universiteit Brussel.

He joined the Miller Group, Stanford University, Stanford, CA, as a Visiting Researcher from 2010 to July 2011. During the M.S. degree, he visited Kungliga Tekniska Högskolan, Stockholm, Sweden, as a Visiting Student in 2009. During that year, he served as a president of the local group of the Board of European Students of Technology, Stockholm. His current research interests include optical interconnects and advanced simulation and optimization methods in nanophotonics.

Mr. Wahl has been a member of the International Society for Optics and Photonics (SPIE) since 2010.

David A. B. Miller (M'83–F'95) received the Ph.D. degree in physics from Heriot-Watt University, Edinburgh, Scotland, U.K., in 1979.

He was with Bell Laboratories, Holmdel, NJ, from 1981 to 1996, as a Department Head from 1987. He is currently the W. M. Keck Professor of electrical engineering and a Co-Director of the Stanford Photonics Research Center, Stanford University, Stanford, CA. He has published more than 230 scientific papers and the text Quantum Mechanics for Scientists and Engineers. He also holds 69 patents. His current research interests include physics and devices in nanophotonics, nanometallics, quantum-well optoelectronics, and fundamentals and applications of optics in information sensing, switching, and processing.

Dr. Miller received numerous awards. He is a fellow of the Optical Society of America, the American Physical Society, and the Royal Societies of Edinburgh and London, holds two honorary degrees, and is a member of the National Academy of Sciences and the National Academy of Engineering.